# Resistor Emulation Approach to Low-Power RF Energy Harvesting

Thurein Paing, *Member, IEEE*, Jason Shin, *Member, IEEE*, Regan Zane, *Senior Member, IEEE*, and Zoya Popovic, *Fellow, IEEE*

***Abstract*—This paper presents an approach and associated circuitry for harvesting near maximum output power from electromagnetic waves in the RF/microwave region of the spectrum with variable incident power densities in the range of tens of $\mu$W/cm$^2$. It is shown that open loop resistor emulation at the input port of a power converter is a suitable solution for tracking the peak power point of a low-power rectifying antenna source over a wide range of incident RF power densities. A boost converter with a simple low-power control approach for resistor emulation is presented. A hardware design example with detailed efficiency analysis is given using commercially available discrete circuitry. Experimental results are presented for a system harvesting 420 $\mu$W to 8 $\mu$W from a 6 cm $\times$ 6 cm rectifying antenna with incident RF power ranging from 70 $\mu$W/cm$^2$ to 30 $\mu$W/cm$^2$, respectively. The results demonstrate that resistor emulation is a simple and practical approach to energy harvesting with variable low-power radiative RF sources.**

***Index Terms*—DC–DC, low power, maximum power point tracking, resistor emulation, RF energy harvesting.**

## I. Introduction

THERE is significant interest in technologies that allow miniature low power wireless devices to operate with low maintenance for extended periods of time [1]–[3]. One approach is to harvest energy from a variety of power sources for extended battery life or battery-less operation [3]. The available power for miniature devices is often very low with variable source output power and impedance due to changes in the environment and mobility of the receiving device. Efficient power management circuits can be used to provide a buffer between the harvesting device and electronic applications. A primary challenge for power management is in maintaining maximum output power from the source over a wide range of operating conditions.

Many techniques are well known for maximum power point tracking (MPPT) and are commonly used in high-power photovoltaic and wind power systems [4]–[16]. Common techniques include perturbation and observation method (P&O) [4]–[7], ripple correlation control (RCC) [8], incremental conductance method (InCond) [9], [10], and fuzzy logic control [11]–[14]. Although the P&O method is among the simplest of the MPPT techniques, it still requires continuous operation of analog and digital hardware to perform calculation of the power level and track the maximum power point (MPP). At the submilliwatt power levels of interest in this paper, very little control overhead is allowable despite a requirement to track the MPP at the rate of anticipated environmental and mobility-related changes in order to harvest appropriate power for device operation. In such low power applications, sources are often connected directly to a battery with shunt and series protection. This approach requires the power source to output a sufficiently high voltage and only results in near peak power operation over a narrow range of input power levels [17]. Boost type switching converters can be used to step-up the output voltage from low voltage power sources. However, traditional output voltage or charge controllers neglect the characteristics of the power source and likely force operation well below the MPP due to the negative input resistance of a voltage regulator.

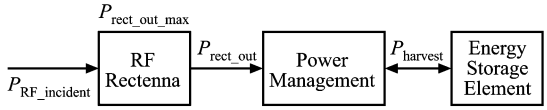


Fig. 1. Radiative RF energy harvesting system block diagram. The antenna or antenna array is integrated with rectifying elements. An incident power density of the electromagnetic waves is absorbed by an effective area of the antenna, and the received power is rectified with some efficiency. The output dc power $P_{\text{rect\_out}}$ is delivered to the energy storage element as $P_{\text{harvest}}$ through an efficient power management circuit.

This paper presents an approach and associated circuitry for harvesting near maximum energy from variable low-power radiative RF sources. The RF sources are known RF power transmitters in a controlled environment whose distances and orientation to the harvesting system can vary. At very low power levels, typical MPPT techniques are not suitable due to the high-power overhead of complex control circuitry. The proposed approach is based on an antenna integrated with rectifying devices, referred to as a rectennas, that achieve by appropriate design [18]–[20], maximum dc output power, $P_{\text{rect\_out\_max}}$, over a wide range of RF incident power densities, $S_{\text{RF}}$, when loaded with a constant resistance. A power converter is realized to act as a constant positive resistance at its input port with minimal control overhead while transferring energy to an output capacitor or battery at voltages appropriate for the sensor load application. The system block diagram is summarized in Fig. 1. The converter operates to match the rectenna characteristics such that $P_{\text{rect\_out\_max}} \approx P_{\text{rect\_out}}$ over a wide range of power density $S_{\text{RF}}$. By emulating a constant resistance matched to the characteristics of the rectenna, the converter does not need to constantly search for the MPP.

Manuscript received July 19, 2007. This work was supported by the RERC on Advancing Cognitive Technologies, U.S. Department of Education NIDRR Grant #H133E040019, and the National Science Foundation (NSF) *SENSORS* project under Grant #0330466. Recommended for publication by Associate Editor S. Pekarek.

The authors are with the Colorado Power Electronics Center (CoPEC), Department of Electrical and Computer Engineering, University of Colorado at Boulder, Boulder, CO 80309-0425 USA (e-mail: thurein.paing@colorado.edu; jason.shin@colorado.edu; zane@colorado.edu; zoya@colorado.edu).

Digital Object Identifier 10.1109/TPEL.2008.921167

0885-8993/$25.00 © 2008 IEEE

Authorized licensed use limited to: UNIVERSITY OF COLORADO. Downloaded on November 13, 2008 at 15:08 from IEEE Xplore. Restrictions apply.

Emphasis in this paper is placed on achieving high converter efficiency at very low $S_{\mathrm{RF}}$ by simplifying control strategies and optimizing the power stage design. Details of the RF rectifying antenna characteristics and energy harvesting requirements are presented in Section II. Analysis of the boost converter as a resistor emulator in the energy harvesting application is given Section III, followed by a converter design example in Section IV. Experimental results are presented in Section V for a complete system harvesting 420 $\mu$W to 8 $\mu$W from a 6 cm $\times$ 6 cm rectifying antenna with incident RF power ranging from 70 $\mu$W/cm$^2$ to 30 $\mu$W/cm$^2$, respectively.

## II. RF Rectifying Characteristics and Energy Harvesting Requirements

Harvesting of radiative RF energy in the system of Fig. 1 can be achieved using rectennas and accompanying power management circuitry, where the goal for power management is to optimally load the rectenna at the dc output to achieve maximum harvested power, $P_{\mathrm{harvest}}$. The appropriate and easily measurable efficiencies within the harvesting system are defined as follows:

Optimal RF-to-DC conversion efficiency

$$\eta_{\mathrm{RF\_conversion}} = \frac{P_{\mathrm{rectenna\_out\_max}}}{P_{\mathrm{RF\_incident}}} \tag{1}$$

where $P_{\mathrm{RF\_incident}} = S_{\mathrm{RF}} \cdot A_{\mathrm{antenna}}$, and $A_{\mathrm{antenna}}$ is defined as the geometric area of the rectenna:

Tracking circuit efficiency

$$\eta_{\mathrm{track}} = \frac{P_{\mathrm{rectenna\_out}}}{P_{\mathrm{rectenna\_out\_max}}} \tag{2}$$

Converter efficiency

$$\eta_{\mathrm{converter}} = \frac{P_{\mathrm{harvest}}}{P_{\mathrm{rect\_out}}} \tag{3}$$

and System efficiency

$$\eta_{\mathrm{system}} = \frac{P_{\mathrm{harvest}}}{P_{\mathrm{RF\_incident}}}. \tag{4}$$

Results demonstrating high efficiency rectification $\eta_{\mathrm{RF\_conversion}}$ at low incident RF power densities, $S_{\mathrm{RF}}$, have been published for both broadband and narrowband transmission with circular and dual linear polarization rectennas in [18]–[20]. An example of a 2.4 GHz dual polarized patch rectenna is shown in Fig. 2(a). Measured rectenna output characteristics are shown in Fig. 2(b) as a function of $S_{\mathrm{RF}}$, indicating that the rectenna is capable of delivering a wide range of output dc currents and voltages. The power curves show that the rectenna peak power point, $P_{\mathrm{rect\_out\_max}}$, over various input power levels can be reached with a constant positive resistance as its load. For the rectenna of Fig. 2(a), this resistance is in the range of 700 $\Omega$–800 $\Omega$. A number of different rectenna types that show similar load behavior have been demonstrated, including a $4 \times 4$ broadband dual-circularly polarized spiral array shown in Fig. 2(c) with dc power output characteristics shown in Fig. 2(d) measured at 2.11 GHz over a range of incident power densities.

The two sets of curves in Fig. 2(b) and (d) show that constant voltage or current control can only result in operation near the MPP, $P_{\mathrm{rect\_out\_max}}$, over a narrow range of incident RF power levels $S_{\mathrm{RF}}$, thus requiring frequent monitoring and control to track $P_{\mathrm{rect\_out\_max}}$ with variable $S_{\mathrm{RF}}$. The same problem arises if the rectenna is connected directly to a battery. The situation is even worse if the rectenna is connected directly to a large capacitor for energy storage due to a time varying capacitor voltage that has no inherent correlation to the MPP. The purpose of the power converter is to match the optimal load resistance of the rectenna at the converter input port and efficiently transfer the energy to its output port based on the voltage and charge characteristics of the energy storage device.

## III. Boost Converter as a Resistor Emulator

The technique applied here is to operate a boost converter as an open-loop resistor emulator, thus allowing the converter to naturally track the rectenna MPP, $P_{\mathrm{rect\_out\_max}}$, with very little control overhead. As seen in Fig. 2(b), once the converter has been tuned to match the optimal load resistance for the rectenna, maximum power can be harvested ($P_{\mathrm{rect\_out\_max}} \approx P_{\mathrm{rect\_out}}$) over a wide range of incident RF power densities $S_{\mathrm{RF}}$ without modifying the converter behavior. The initial tuning operation to set the converter emulated resistance could be performed once in the manufacturing process or as an infrequent recalibration procedure.

Resistor emulation techniques have been used previously, most commonly in power-factor correction (PFC) applications. Some approaches for PFC at lower current levels are based on converters with natural resistor emulation at the input port (without current feedback), including boost type converters in critical conduction mode (CRM) and buck-boost type converters in discontinuous conduction mode (DCM) [21]. At higher current levels, most PFC circuits operate in continuous conduction mode (CCM) with more advanced current and voltage feedback control [21]. The natural emulation techniques and approximations to them are used in this work to achieve resistor emulation with low power, essentially open-loop, control circuitry.

A boost topology is selected, as shown in Fig. 3(a), due to the low output voltage of the rectenna source (input voltage, $V_{\mathrm{in}}$, to converter). The inductor current waveform is shown in Fig. 3(b) when operated in DCM with an on-time, $t_1$, of $Q_1$ and constant frequency, $1/T_{\mathrm{hf}}$. The converter is run in a pulsed mode with a low frequency pulse duty cycle, $k$, and period, $T_{\mathrm{lf}}$. The majority of the control circuitry is completely shut down when the converter is not active in order to reduce control losses. A diode rectifier is used as opposed to a synchronous rectifier to reduce control losses by removing the need for an amplifier to detect inductor current zero-crossings or for self-excitation as in [22] and [23]. Given this mode of operation, the converter parameters are: $t_1, T_{\mathrm{hf}}, L$, and $k$. By averaging over $T_{\mathrm{lf}}$, the low-frequency emulated resistance at the input port of the converter is given by

$$R_{\mathrm{em}} = \frac{V_{\mathrm{in}}^2}{P_{\mathrm{in}}} = \frac{2 \cdot L \cdot T_{\mathrm{hf}}}{t_1^2 \cdot k}\left(\frac{M-1}{M}\right), \quad \text{where } M = \frac{V_o}{V_{\mathrm{in}}}. \tag{5}$$

Note that (5) includes a term with the converter conversion ratio $M$. This is undesirable since the emulated resistance should ideally be independent of $V_{\mathrm{in}}$ and $V_o$. However, if the converter has

Authorized licensed use limited to: UNIVERSITY OF COLORADO. Downloaded on November 13, 2008 at 15:08 from IEEE Xplore. Restrictions apply.

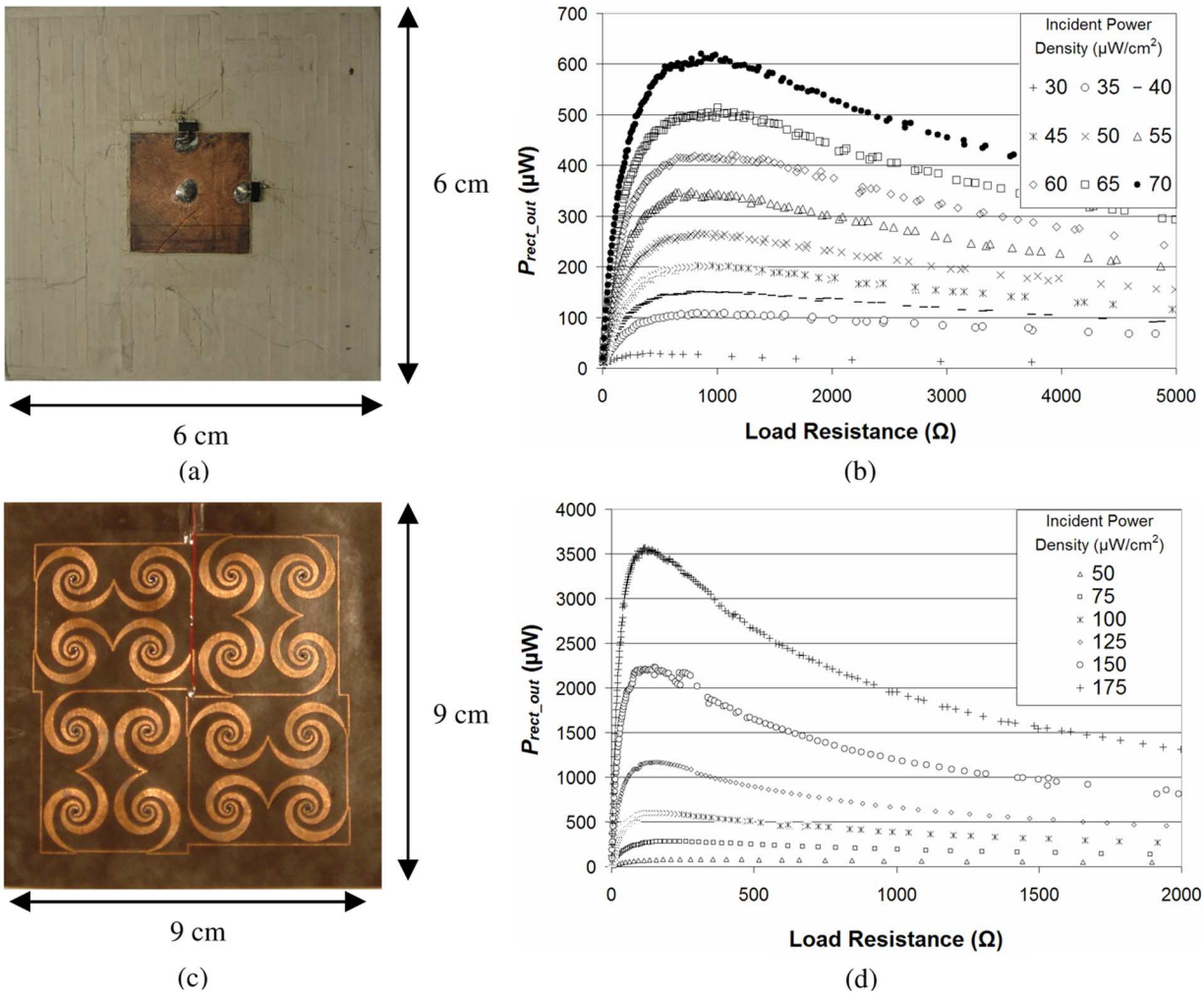


Fig. 2. (a) Photograph of a 2.4-GHz dual-polarized patch rectenna backed by a ground plane. Two Schottky diodes rectify independently the two linear orthogonal wave polarizations, and the RF null of the patch antenna is used to place the metallized via which is the dc output. (b) Measured power curves of the patch rectenna over a range of incident power densities. (c) Photograph of a broadband (2–18 GHz) dual circularly polarized spiral rectenna array fabricated on a flexible substrate with no ground plane. (d) Measured dc power curves of the spiral rectenna array show very similar load characteristics to the patch rectenna.

a large step-up conversion ratio ($V_{\rm in} \ll V_o$), then the correction factor, $(M-1)/M$, is approximately unity, and the $R_{\rm em}$ equation reduces to an equation that does not depend on $V_{\rm in}$ or $V_o$. Similar relationships are given in [24] for operation in variable frequency CRM to achieve resistor emulation with no dependence on $M$ at the expense of additional control circuitry. Suitable control approaches are also given in [24] for buck and buck-boost type converters. An example of using a buck converter in constant duty cycle DCM for piezoelectric energy harvesting applications is given in [25], which also exhibits resistor emulation for high step down ratios as shown in [24]. A similar example using a buck-boost converter is given in [26].

For design optimization of the boost converter, equations predicting converter power losses are first derived. These equations are then used to find the optimum values of $L, t_1, T_{\rm hf}$ and $k$ that maximize converter efficiency while limiting the required input capacitance. The power losses are grouped into control, conduction and switching losses, as shown below

$$P_{\rm loss} = P_{\rm cond} + P_{\rm sw} + P_{\rm ctrl}$$
$$P_{\rm ctrl} = P_{\rm fix}(k, f_{\rm lf}) + P_{\rm pwm}(f_{\rm hf}) \cdot \left(k + \frac{t_{\rm settle}}{T_{\rm lf}}\right) \quad (6)$$

$$P_{\rm cond} = \left(R_{l,\rm esr}\left(I_{L,\rm rms1}^2 + I_{L,\rm rms2}^2\right) + R_{\rm on} \cdot I_{L,\rm rms1}^2 + V_D \cdot I_{L,\rm avg2}\right) \cdot k \quad (7)$$

$$P_{\rm sw} = \left(Q_g \frac{V_o}{2} + C_{\rm oss}\frac{V_{\rm in}^2}{2}\right) \cdot \frac{1}{T_{\rm hf}} \cdot k \quad (8)$$

where the RMS, average, and peak currents and high-frequency period are defined as

$$I_{L,\rm rms1} = I_{\rm pk}\sqrt{\frac{t_1}{3T_{\rm hf}}}$$
$$I_{L,\rm rms2} = I_{\rm pk}\sqrt{\frac{V_{\rm in}}{V_o - V_{\rm in}}}\sqrt{\frac{t_1}{3T_{\rm hf}}}$$
$$I_{L,\rm avg2} = I_{\rm pk}\frac{V_{\rm in}}{V_o - V_{\rm in}}\frac{t_1}{2T_{\rm hf}},$$
$$I_{\rm pk} = \frac{V_{\rm in}}{L}t_1, \quad T_{\rm hf} = \left(1 + \frac{V_{\rm in}}{V_o - V_{\rm in}}\right) \cdot t_1. \quad (9)$$

Within the control losses, $P_{\rm fix}$ is the power consumption of the control circuitry that is constantly operating (e.g., the low-frequency oscillator controlling the pulsing duty cycle $k$). The power loss included in $P_{\rm pwm}$ is the power consumption of the

Authorized licensed use limited to: UNIVERSITY OF COLORADO. Downloaded on November 13, 2008 at 15:08 from IEEE Xplore. Restrictions apply.

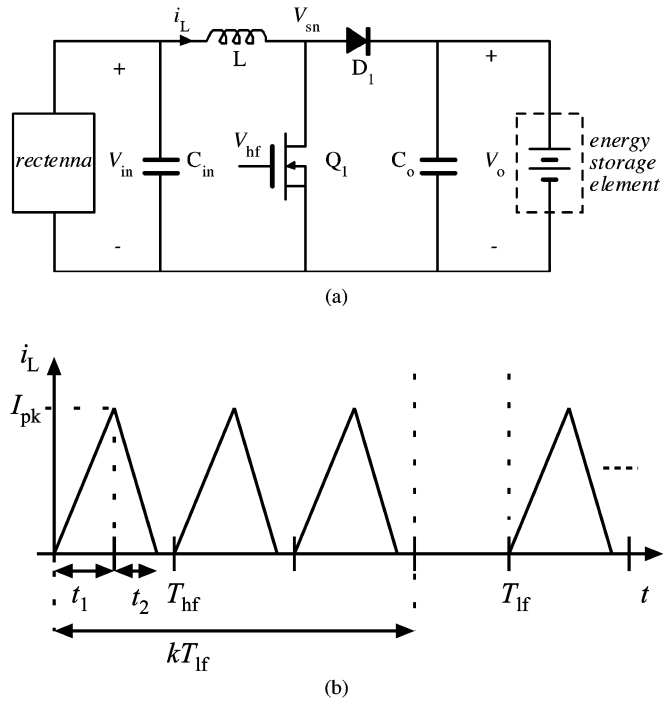


Fig. 3. (a) Boost converter topology. (b) Inductor current waveform in fixed-frequency DCM. $T_{\rm hf}$ and $T_{\rm lf}$ are the high- and low-frequency periods, respectively. $kT_{\rm lf}$ is the duration of the pulsed operation. $t_1$ and $t_2$ are the primary and secondary switch intervals, respectively.

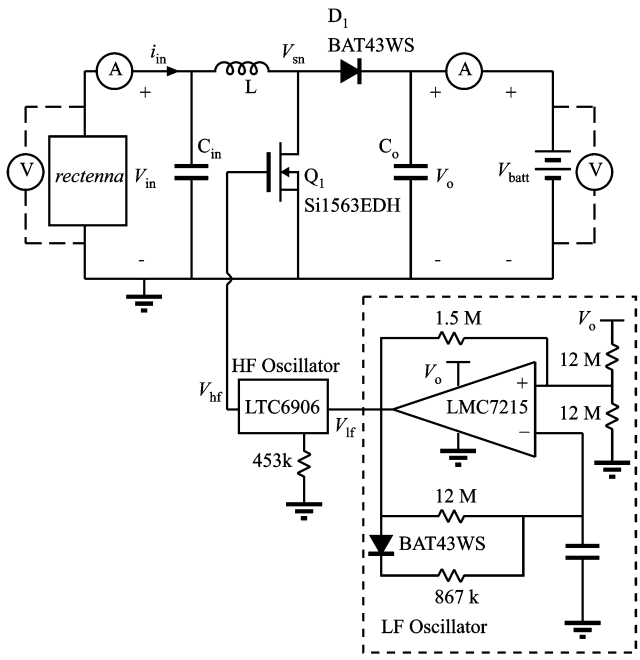


Fig. 4. Schematic of discrete transistor-diode boost converter. Control circuitry consists of a LF oscillator that directly powers the HF oscillator. The HF oscillator output drives the N-Channel MOSFET $Q_1$.

TABLE I
COMPONENTS USED IN BOOST DESIGN

| Component | Part no. | Comments |
|---|---|---|
| MOSFET (N-Channel in complementary package) | Si1563EDH | $R_{on}$ = 0.344 Ω<br>$Q_g$ = 650 pC<br>$C_{oss}$ = 35 pF |
| Schottky Diode | BAT43WS | $V_d$ = 0.26 V |
| HF Oscillator | LTC6906 | $I_{ss}$ = 12 μA (@ 100 kHz) |
| LF Oscillator Comparator | LMC7215 | $I_{ss}$ = 0.7 μA |
| Inductor | DS1608C series | $R_{l,esr} \approx 6 \times 10^3 \times L$ |

control circuitry that is enabled and disabled as the converter is pulsed. Therefore, $P_{\rm pwm}$ is multiplied by $(k + t_{\rm settle}/T_{\rm lf})$. The $t_{\rm settle}$ term is the time required for the pulsed control circuitry to settle after it has been enabled. The conduction and switching losses are also multiplied by $k$ as the converter is only in operation during $kT_{\rm lf}$. $R_{l,\rm esr}$ is the inductor series resistance. The switching losses associated with the MOSFET gate-to-drain capacitance $C_{\rm gd}$ are neglected since the off-state drain voltage $V_{\rm in}$ is typically only a few hundred millivolts. Due to the simple open-loop operation, low power control circuitry can be used to achieve the primary functions of a high-frequency (HF) oscillator to drive the MOSFET and a low-frequency (LF) oscillator to set $k$.

## IV. ENERGY HARVESTER DESIGN EXAMPLE

The choice of parameter settings for the given converter is based on the expected range of input power levels, desired emulated resistance, and output voltage. A power converter design example is given here together with details on each of the major design steps for providing an interface between the patch rectenna of Fig. 2(a) with output characteristics shown in Fig. 2(b) and a 4.2-V thin-film battery. The schematic for the boost converter built with commercially available components is shown in Fig. 4 along with the experimental meter configuration used in gathering experimental results presented in Section V. Details on the components used in the design are given in Table I.

### A. Selection of Control Components

To control the converter, an HF oscillator and an LF oscillator are used with emphasis on the selection of components with the lowest power consumption. The HF resistor-set oscillator (LTC6906) has a fixed duty cycle (50%). This duty cycle ensures DCM operation for $V_o/V_{\rm in} > 2$. When powered on at the beginning of each LF period, there is a settling time $t_{\rm settle}$ before the output of the oscillator is enabled. This output drives the MOSFET in the converter. Therefore, adjusting the frequency, $1/T_{\rm hf}$, changes the value of $t_1 = T_{\rm hf}/2$ and thus the emulated resistance seen by the input source. The power consumption of the LTC6906 HF oscillator is the value used as $P_{\rm pwm}$ in the power loss calculations in (6). To perform the pulsing operation of the converter, a LF oscillator is built around a low power comparator (LMC7215). This oscillator has an adjustable positive duty cycle $D_{\rm lf}$ that affects the $k$ parameter (5). The HF oscillator is directly powered from the LF oscillator output. The boost converter is in operation during $kT_{\rm lf} = D_{\rm lf}T_{\rm lf} - t_{\rm settle}$.

### B. Selection of L

Given a converter input power level $P_{\rm rect\_out}$, changes in power loss are calculated from (6) to (9) as $L$ and $t_1$ are swept over a range of values and $k$ is solved for so that the approximate

Authorized licensed use limited to: UNIVERSITY OF COLORADO. Downloaded on November 13, 2008 at 15:08 from IEEE Xplore. Restrictions apply.

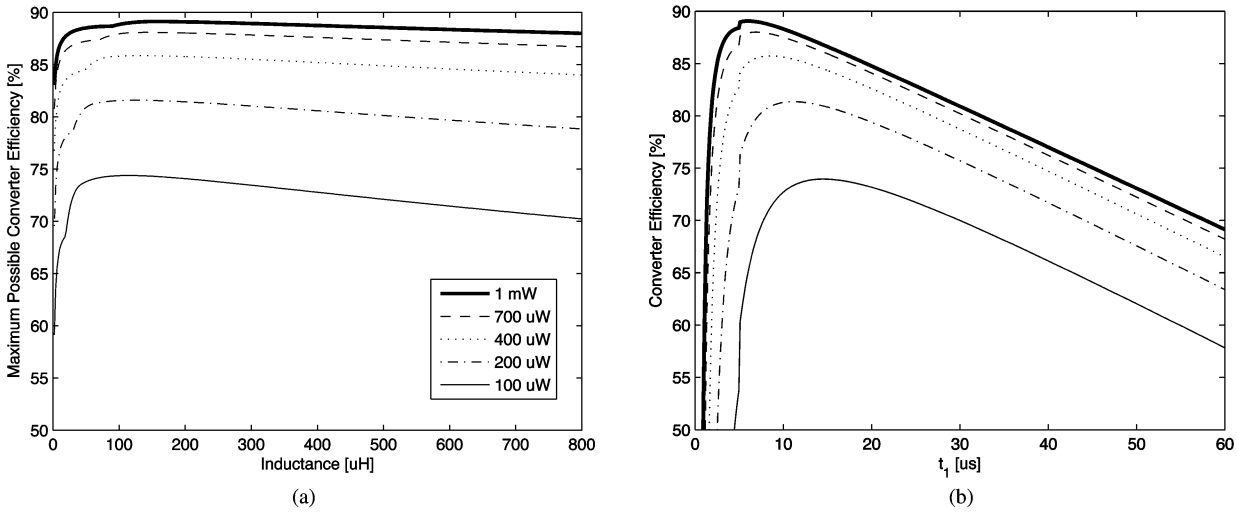


Fig. 5. Simulations at multiple converter input power levels, $P_{\mathrm{rect\_out}}$ for: (a) maximum possible converter efficiency $\eta_{\mathrm{converter}}$ as a function of L, and (b) estimated $\eta_{\mathrm{converter}}$ as a function of $t_1$ with fixed $L = 220\ \mu$H.

desired $R_{\mathrm{em}} = 750\ \Omega$ is achieved. In (7), $R_{l,\mathrm{esr}}$ is a function of inductance value following Table I. After these simulations are run at different power levels, the converter efficiency, $\eta_{\mathrm{converter}}$, is analyzed as a function of $t_1$ and $L$. Fig. 5(a) shows a plot of the maximum achievable efficiency as a function of $L$, with $t_1$ solved at each point to achieve maximum efficiency. The family of plots in Fig. 5(a) show that an inductance value in the range of 100 $\mu$H to 200 $\mu$H is optimal. Therefore, an inductance of $L$ = 220 $\mu$H is selected for this converter design (based on available discrete components).

### C. Selection of $t_1$ and $k$

Next, the calculations are rerun with the fixed $L$ to select the appropriate $t_1$, as shown in Fig. 5(b). The value of $k$ is then determined by the desired $R_{\mathrm{em}}$. The selection is optimized for the lower power levels due to the emphasis of this work on demonstrating RF energy harvesting at very low $S_{\mathrm{RF}}$. Parameters $t_1$ and $k$ are chosen to be 18 $\mu$s and 0.06, respectively.

### D. Selection of Input Filter Capacitance

Although the frequency of the LF oscillator does not affect the value of the emulated resistance, it does determine the size of the input filter capacitor required to meet a voltage ripple $\Delta v_{\mathrm{in}}$ specification. This dependence is expressed in the following equation (assuming 50% HF duty cycle as in this design):

$$C_{\mathrm{in\_min}} = \left(\frac{t_1 \cdot k \cdot T_{\mathrm{lf}}}{4 \cdot L}\right) \cdot \left(\frac{V_{\mathrm{in}}}{\Delta v_{\mathrm{in}}}\right). \tag{10}$$

The ability of a wireless power source to supply instantaneous current is limited. Therefore, most of the instantaneous energy supplied to the converter during high-frequency switching transitions comes from the input filter capacitor. Due to this constraint, $T_{\mathrm{lf}}$ has to be included in the design considerations. Note from (6) that $P_{\mathrm{fix}}$ and $P_{\mathrm{pwm}}$ are power losses that are functions of the oscillation frequency and positive duty cycle. Thus, $t_{\mathrm{settle}}$ sets a limit on how small the low-frequency period $T_{\mathrm{lf}}$ can be. With these considerations in mind, there is tradeoff between the choice of $T_{\mathrm{lf}}, C_{\mathrm{in}}$, and acceptable $P_{\mathrm{ctrl}}$ given an allowable

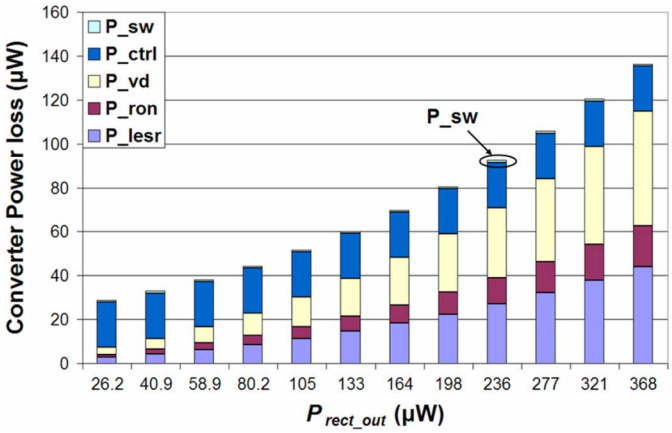


Fig. 6. Power loss distribution of transistor-diode boost converter at a range of input power levels to the converter from the rectenna, $P_{\mathrm{rect\_out}}$.

percentage voltage ripple, $\Delta v_{\mathrm{in}}/V_{\mathrm{in}}$ selected for the design, as shown in (10). Note that large input voltage ripple may cause the power source to operate away from the MPP for a significant portion of $T_{\mathrm{lf}}$.

Fig. 6 shows a chart of the loss budget of the transistor-diode boost converter with the selected parameter values. As expected, the conduction losses dominate at the higher input power levels due to the increased currents, and control losses dominate at the lower input power levels. Of the three conduction loss components, $P_{\mathrm{ron}}$ (transistor on-state resistance), $P_{l,\mathrm{esr}}$ (inductor equivalent series resistance), and $P_{vd}$ (diode forward voltage), the diode forward voltage is the main cause of the power losses. However, $P_{vd}$ is not sufficiently high at the lower power levels to justify the additional control losses that would be introduced by using a synchronous rectifier. $P_{\mathrm{ctrl}}$ is fixed and is approximately 20 $\mu$W.

## V. Experimental Results

The RF energy harvesting system shown in Fig. 4 was built and tested using the components from Table I, the 2.4-GHz

Authorized licensed use limited to: UNIVERSITY OF COLORADO. Downloaded on November 13, 2008 at 15:08 from IEEE Xplore. Restrictions apply.

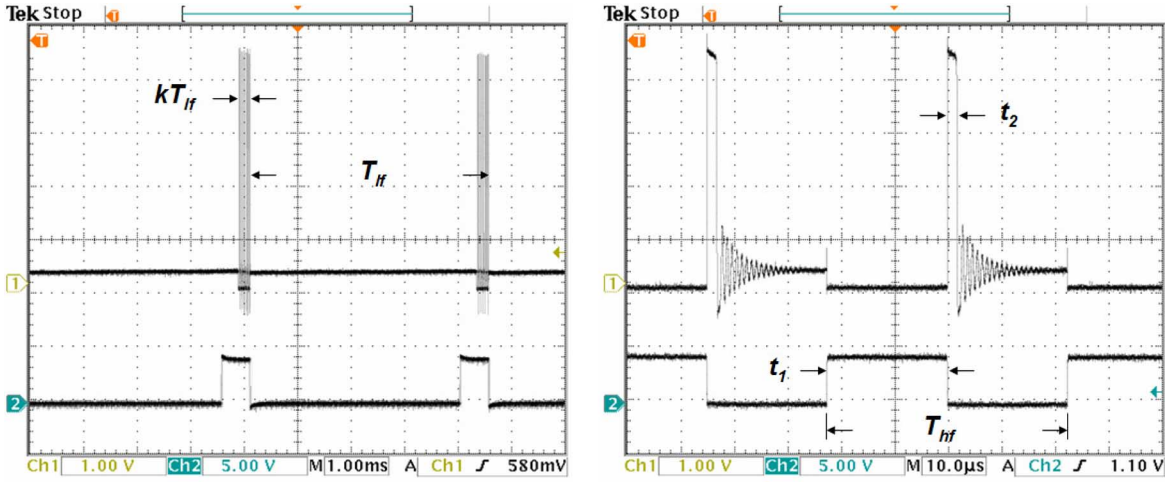


(a) (b)

Fig. 7. Experimental boost converter results at $S_{\rm RF} = 50\ \mu$W/cm$^2$, $V_{\rm in} = 0.44$ V, $V_o = 4.15$ V. (a) Ch1—Switch-node voltage waveform $V_{\rm sn}$. Ch2—LF oscillator output $V_{\rm lf}$. (b) Ch1—Switch-node voltage waveform $V_{\rm sn}$. Ch2—Q1 gate-drive waveform (HF oscillator output $V_{\rm hf}$).

TABLE II
BOOST EXPERIMENTAL RESULTS WITH RECTENNA

| $S_{RF}$ ($\mu$W/cm$^2$) | $\eta_{RF\_conversion}$ (%) | $\eta_{track}$ (%) | $\eta_{converter}$ (%) | $\eta_{system}$ (%) | $M = V_o/V_{in}$ ($V_o$ = 4.15 V) | $P_{harvest}$ ($\mu$W) |
|---|---|---|---|---|---|---|
| 30 | 2.5 | 85 | 36.2 | 0.8 | 30.7 | 8.3 |
| 35 | 8.6 | 86.4 | 53.8 | 4.0 | 15.3 | 50.2 |
| 40 | 10.5 | 86.1 | 65.4 | 5.9 | 12.9 | 85.1 |
| 45 | 12.4 | 90.1 | 69.2 | 7.7 | 10.9 | 125.3 |
| 50 | 14.7 | 92.8 | 70.2 | 9.6 | 9.4 | 172.6 |
| 55 | 17.4 | 89.5 | 73.8 | 11.5 | 8.4 | 227.8 |
| 60 | 19.3 | 90.3 | 74.7 | 13.0 | 7.7 | 281.4 |
| 65 | 21.6 | 90.7 | 75.6 | 14.8 | 7.0 | 346.5 |
| 70 | 24.6 | 87.9 | 77.1 | 16.7 | 6.4 | 420.0 |

dual polarized patch rectenna shown in Fig. 2(a), and a 4.2-V, 400-$\mu$Ah thin-film battery from Front Edge Technologies. The battery was selected for its small form factor, trickle charge capability, and low leakage. The presence of the battery fixes the output voltage, $V_o$ (measured at $V_o = V_{\rm batt} = 4.15$ V during experimentation). The converter parameters are: $1/T_{\rm lf} = 250$ Hz, $C_{\rm in} = 20\ \mu$F, $\Delta v_{\rm in}/V_{\rm in} = 20\%, L = 220\ \mu$H, $t_1 = 22.4\ \mu$s, and $k = 0.0483$. Note that the values for $t_1$ and $k$ are slightly different than the design optimization due to the inability to precisely set $k$ and an accompanying $t_1$ with available low power discrete components. Revisiting Fig. 5(b), there is a minimal decrease in expected efficiency due to the new $t_1$. The limitations are due to the selection of $C_{\rm in}$ and the corresponding $T_{\rm lf}$ requirement to achieve an acceptable input voltage ripple.

The converter is tested over a range of far-field RF input power densities $S_{\rm RF}$ by sweeping the transmitted RF power to the rectenna using a calibrated setup in an anechoic chamber. High precision, calibrated multimeters (Agilent 34411A) are used to measure the input and output voltages and currents of the boost converter as shown by the voltmeter and ammeter symbols in Fig. 4. The output current is measured as shown between $V_o$ and $V_{\rm batt}$ and the controller is powered from $V_o$. Therefore, the measured output power, $P_{\rm harvest}$, is the total harvested output power taking into account all losses in the control circuitry.

Fig. 7 shows captured oscilloscope waveforms of the switch-node voltage, $V_{\rm sn}$, the LF oscillator output, $V_{\rm lf}$, and the HF oscillator output $V_{\rm hf}$ of the converter at $S_{\rm RF} = 50\ \mu$W/cm$^2$. Note that the HF oscillator settling time $t_{\rm settle}$ is about the same length as $kT_{\rm lf}$ at the operating point in Fig. 7, which limits the ability to reduce control losses $P_{\rm ctrl}$ at low $k$ values as shown in (6). The ringing in $V_{\rm sn}$ seen in Fig. 7(b) shows a small additional switching loss associated with reverse recovery of the diode $D_1$ when operating in DCM. Switching losses due to $C_{\rm gd}$ are negligible in DCM due to the low value of $V_{\rm in}$.

Experimental results are tabulated in Table II with Fig. 8 showing a plot of $\eta_{\rm converter}$ and $P_{\rm harvest}$ versus $S_{\rm RF}$. The emulated resistance behaves as desired and the converter achieves a tracking efficiency $\eta_{\rm track}$ between 85%–92.8%. The discrete circuitry prevents finer tuning of the emulated resistance and thus a higher $\eta_{\rm track}$. It is worth noting that at the lowest input power of $P_{\rm rect_out} = 22.95\ \mu$W (corresponding to $\sim$30 $\mu$W/cm$^2$ incident RF power density), the system is still able to harvest 8.3 $\mu$W to trickle charge the battery (with $V_{\rm batt} = 4.15$ V). Use of the harvesting system presented here in a wireless sensor application is presented in [27], demonstrating operation of a wireless patient activity level monitor that samples and transmits temperature, skin resistance and three-axis motion and position at variable sample intervals based on available power from the harvester. At the slowest

Authorized licensed use limited to: UNIVERSITY OF COLORADO. Downloaded on November 13, 2008 at 15:08 from IEEE Xplore. Restrictions apply.

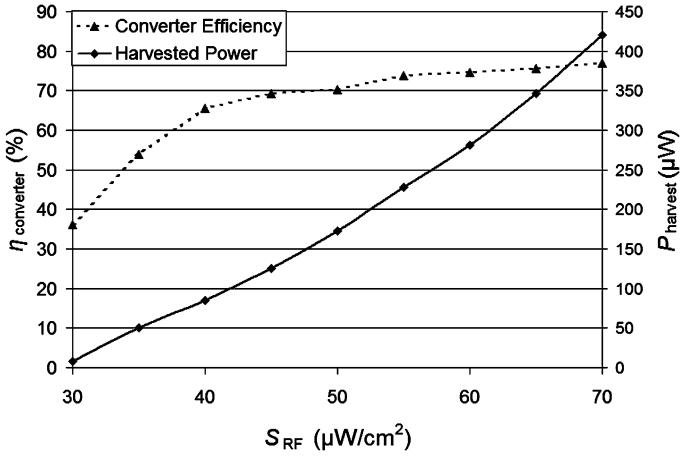


Fig. 8. Experimental results of converter efficiency ($\eta_{\rm harvest}$) and power harvested by the system ($P_{\rm harvest}$) as a function of incident RF power density ($S_{\rm RF}$).

sampling rates (sample intervals greater than 10 s), the wireless monitor requires less than 5 $\mu$W for reliable operation.

## VI. Conclusion

Low-power RF rectennas are shown to exhibit maximum power points at near constant optimal dc load resistance over a decade of output power, $P_{\rm rect\_out}$. A boost converter topology operating in open-loop fixed-frequency DCM is used to achieve near constant emulated resistance with simple open-loop control based on low-power timing circuits. The converter control variables, $t_1, k, L, f_{\rm lf}$, and $C_{\rm in}$ are selected based on a detailed efficiency analysis to minimize power losses and achieve the desired emulated resistance. Experimental results are presented for an RF energy harvesting system comprising a 2.4-GHz dual linearly polarized 6 cm $\times$ 6 cm patch rectenna, boost converter and controller designed with commercially available components, and a 4.2-V thin-film Lithium battery. The results demonstrate system operation with $P_{\rm harvest}$ ranging from 420 $\mu$W to 8 $\mu$W for a rectenna output $P_{\rm rect\_out}$ ranging from 545 $\mu$W to 23 $\mu$W, respectively. Tracking efficiencies of 85%–92.8% are achieved over the full range of $P_{\rm rect\_out}$. The proposed resistor emulation approach to low-power energy harvesting provides a simple solution for maximizing output power in harvesting applications with variable source power.

## References

[1] Q. Dong, "Maximizing system lifetime in wireless sensor networks," in *Proc. 4th Int. Conf. Info. Process. Sens. Netw. (IPSN'05)*, Los Angeles, CA, Apr. 2005, pp. 13–19.

[2] Q. Cao, T. Abdelzaher, T. He, and J. Stankovic, "Towards optimal sleep scheduling in sensor networks for rare-event detection," in *Proc. 4th Int. Conf. Inf. Process. Sens. Netw. (IPSN'05)*, Los Angeles, CA, Apr. 2005, pp. 20–27.

[3] S. Roundy, P. Wright, and J. Rabaey, *Energy Scavenging for Wireless Sensor Networks*. Boston, MA: Kluwer, 2004.

[4] X. Liu and L. A. C. Lopes, "An improved perturbation and observation maximum power point tracking algorithm for PV arrays," in *Proc. IEEE 35th Power Electron. Spec. Conf.*, Aachen, Germany, Jun. 2004, vol. 3, pp. 2005–2010.

[5] N. Femia, G. Petrone, G. Spagnuolo, and M. Vitelli, "Optimization of perturb and observe maximum power point tracking method," *IEEE Trans. Power Electron.*, vol. 20, no. 4, pp. 963–973, Jul. 2005.

[6] S. Jain and V. Agarwal, "A new algorithm for rapid tracking of approximate maximum power point in photovoltaic systems," *IEEE Power Electron. Lett.*, vol. 2, no. 1, pp. 16–19, Mar. 2004.

[7] A. Pandey, N. Dasgupta, and A. K. Mukerjee, "A simple single-sensor MPPT algorithm," *IEEE Trans. Power Electron.*, vol. 22, no. 2, pp. 698–700, Mar. 2007.

[8] T. Esram, J. W. Kimball, P. T. Krein, P. L. Chapman, and P. Midya, "Dynamic maximum power point tracking of photovoltaic arrays using ripple correlation control," *IEEE Trans. Power Electron.*, vol. 21, no. 5, pp. 1282–1291, Sep. 2006.

[9] E. Roman, R. Alonso, P. Ibanez, S. Elorduizapatarietxe, and D. Goitia, "Intelligent PV module for grid-connected PV systems," *IEEE Trans. Ind. Electron.*, vol. 53, no. 4, pp. 1066–1073, Jun. 2006.

[10] E. Koutroulis, K. Kalaitzakis, and N. C. Voulgaris, "Development of a microcontroller-based, photovoltaic maximum power point tracking control system," *IEEE Trans. Power Electron.*, vol. 16, no. 1, pp. 46–54, Jan. 2001.

[11] B. M. Wilamowski and L. Xiangli, "Fuzzy system based maximum power point tracking for PV system," in *Proc. IEEE 28th Conf. Ind. Electron. Soc. (IECON'02)*, Sevilla, Spain, Nov. 2002, vol. 4, pp. 3280–3284.

[12] N. S. D'Souza, L. A. C. Lopes, and X. Liu, "Peak current control based maximum power point trackers for faster transient responses," in *Proc. 16th Can. Conf. Elect. Comput. Eng.*, Ottawa, ON, Canada, May 2006, pp. 659–663.

[13] A. B. Raju, B. G. Fernandes, and K. Chatterjee, "A UPF power conditioner with maximum power point tracker for grid connected variable speed wind energy conversion system," in *Proc. 1st Int. Conf. Power Electron. Syst. Appl.*, Nov. 2004, pp. 107–112.

[14] R. Datta and V. T. Ranganathan, "A method of tracking the peak power points for a variable speed wind energy conversion system," *IEEE Trans. Energy. Conv.*, vol. 18, no. 1, pp. 163–168, Mar. 2003.

[15] E. V. Solodovnik, S. Liu, and R. A. Dougal, "Power controller design for maximum power tracking in solar installations," *IEEE Trans. Power Electron.*, vol. 19, no. 5, pp. 1295–1304, Sep. 2004.

[16] K. K. Tse, M. T. Ho, H. S.-H. Chung, and S. Y. Hui, "A novel maximum power point tracker for PV panels using switching frequency modulation," *IEEE Trans. Power Electron.*, vol. 17, no. 6, pp. 980–989, Nov. 2002.

[17] D. A. Bennett, R. H. Selfridge, J. N. Harb, and D. T. Comer, "A control circuit for a microsensor hybrid power supply," *IEEE Trans. Ind. Electron.*, vol. 51, no. 1, pp. 74–80, Feb. 2004.

[18] J. A. Hagerty and Z. B. Popovic, "An experimental and theoretical characterization of a broadband arbitrarily polarized rectenna array," in *Proc. IEEE MTT-S Int. Micro. Symp. Dig.*, Phoenix, AZ, May 2001, pp. 1855–1858.

[19] J. A. Hagerty, F. B. Helmbrecht, W. H. McCalpin, R. A. Zane, and Z. B. Popovic, "Recycling ambient microwave energy with broad-band rectenna arrays," *IEEE Trans. Microw. Theory. Tech.*, vol. 52, no. 3, pp. 1014–1024, Mar. 2004.

[20] C. Walsh, S. Rondineau, M. Jankovic, G. Zhao, and Z. A. Popovic, "Conformal 10 GHz rectenna for wireless powering of piezoelectric sensor electronics," in *Proc. IEEE MTT-S Int. Microw. Symp.*, Long Beach, CA, Jun. 2005, pp. 1–4.

[21] R. W. Erickson and D. Maksimović, *Fundamentals of Power Electronics*, 2nd ed. New York: Springer, 2001, pp. 637–663.

[22] P. Niu and P. Chapman, "Design and performance of linear biomechanical energy conversion devices," in *Proc. IEEE 37th Power Electron. Spec. Conf.*, Jeju, Korea, Jun. 2006, pp. 1–6.

[23] J. Han, A. von Jouanne, T. Le, K. Mayaram, and T. S. Fiez, "Novel power conditioning circuits for piezoelectric micropower generators," in *Proc. IEEE 19th Appl. Power Electron Conf.*, Anaheim, CA, Feb. 2004, pp. 1541–1546.

[24] T. S. Paing and R. A. Zane, "Resistor emulation approach to low power energy harvesting," in *Proc. IEEE 37th Power Electron. Spec. Conf.*, Jeju, Korea, Jun. 2006, pp. 1–7.

[25] G. K. Ottman, H. F. Hofmann, A. C. Bhatt, and G. A. Lesieutre, "Adaptive piezoelectric energy harvesting circuit for wireless remote power supply," *IEEE Trans. Power Electron.*, vol. 17, no. 5, pp. 669–676, Sep. 2002.

[26] E. Lefeuvre, D. Audigier, C. Richard, and D. Guyomar, "Buck-boost converter for sensorless power optimization of piezoelectric energy harvester," *IEEE Trans. Power Electron.*, vol. 22, no. 5, pp. 2018–2025, Sep. 2007.

[27] T. S. Paing, J. Morroni, A. Dolgov, J. Shin, J. Brannan, R. A. Zane, and Z. B. Popovic, "Wirelessly-powered wireless sensor platform," in *Proc. IEEE 37th Eur. Microw. Conf.*, Munich, Germany, Oct. 2007, pp. 1–4.

Authorized licensed use limited to: UNIVERSITY OF COLORADO. Downloaded on November 13, 2008 at 15:08 from IEEE Xplore. Restrictions apply.

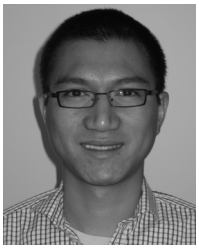

**Thurein Paing** (M'08) received the B.S./M.S. degree in electrical engineering from The Johns Hopkins University, Baltimore, MD, in 2004. He is currently pursuing the Ph.D. degree in electrical engineering at the University of Colorado, Boulder.

His current research interests include power electronics for harvesting energy from wireless power sources and low-power mixed-signal integrated circuit design.

**Jason Shin** (M'06) received the B.S. degree in electrical engineering from the University of Colorado, Boulder, in 2006. He is currently pursuing the M.S. degree in electrical engineering at the University of Colorado, Boulder. His current research interests include rectifier integration in low-power rectenna design.

**Regan Zane** (SM'07) received the B.S, M.S., and Ph.D. degrees in electrical engineering from the University of Colorado, Boulder, in 1996, 1998, and 1999, respectively.

He is currently an Associate Professor of electrical engineering at the University of Colorado, Boulder. From 1999 to 2001, he worked as a Senior Research Engineer at the GE Global Research Center in Niskayuna, NY. At GE, he developed custom integrated circuit controllers for power management in electronic ballasts and lighting systems. In 2001, he joined the University of Colorado as a faculty member, where he has ongoing research programs in energy-efficient lighting systems, adaptive and robust power management systems, and low-power energy harvesting for wireless sensors.

Dr. Zane received the NSF Career Award in 2004 for his work in energy efficient lighting systems, the 2005 IEEE Microwave Best Paper Prize, the University of Colorado 2006 Inventor of the Year award, and 2006 Provost Faculty Achievement award. He currently serves as Associate Editor for the IEEE TRANSACTIONS ON POWER ELECTRONICS.

**Zoya Popovic** ( F'02) received the Dipl.Ing. degree from the University of Belgrade, Serbia, Yugoslavia, in 1985, and the Ph.D. degree from the California Institute of Technology, Pasadena, in 1990.

Since 1990, she has been with the University of Colorado, Boulder, where she is currently the Hudson Moore Jr. Chaired Professor of Electrical and Computer Engineering. She was a Visiting Professor at the Technical University of Munich, Munich, Germany, in 2001. Since 1991, she has graduated 22 Ph.D. students and currently advises a group of 16 graduate students. Her research interests include high-efficiency, low-noise and broadband microwave and millimeter-wave circuits, quasi-optical millimeter-wave techniques for imaging, smart and multibeam antenna arrays, intelligent RF front ends, RF optics, and wireless powering for batteryless sensors.

Dr. Popovic is the recipient of the 1993 and 2006 Microwave Prizes presented by the IEEE Microwave Theory and Techniques Society (IEEE MTT-S) for the best journal papers. She was the recipient of the 1996 URSI Issac Koga Gold Medal. In 1997, Eta Kappa Nu students chose her as a Professor of the Year. She was the recipient of a 2000 Humboldt Research Award for Senior U.S. Scientists from the German Alexander von Humboldt Stiftung. She was also awarded the 2001 Hewelett-Packard (HP)/American Society for Engineering Education (ASEE) Terman Medal for combined teaching and research excellence. She currently serves as the Associate Editor for the IEEE TRANSACTIONS ON MICROWAVE THEORY AND TECHNIQUES.

Authorized licensed use limited to: UNIVERSITY OF COLORADO. Downloaded on November 13, 2008 at 15:08 from IEEE Xplore. Restrictions apply.